Infrared anomalous Hall effect in $SrRuO_3$: Exploring evidence for crossover to intrinsic behavior

M.-H. Kim,[1] G. Acbas,[1] M.-H. Yang,[1] M. Eginligil,[1] P. Khalifah,[2] I. Ohkubo,[3] H. Christen,[4] D. Mandrus,[4] Z. Fang,[5] and J. Cerne[1]

[1]*Department of Physics, University at Buffalo, The State University of New York, Buffalo, New York 14260, USA*

[2]*Department of Chemistry, Stony Brook University, Stony Brook, New York 11794, USA*

[3]*Department of Applied Chemistry, University of Tokyo, Tokyo, Japan*

[4]*Condensed Matter Sciences Division, Oak Ridge National Laboratory, Oak Ridge, Tennessee 37831, USA*

[5]*Institute of Physics, Chinese Academy of Science, Beijing 100080, China*

(Received 28 October 2009; revised manuscript received 12 April 2010; published 30 June 2010)

The origin of the Hall effect in many itinerant ferromagnets is still not resolved with an anomalous contribution from the sample magnetization that can exhibit extrinsic or intrinsic behavior. We report the midinfrared (MIR) measurements of the complex Hall (θ_H), Faraday (θ_F), and Kerr (θ_K) angles, as well as the Hall conductivity (σ_{xy}) in a $SrRuO_3$ film in the 115–1400 meV energy range. The magnetic field, temperature, and frequency dependence of the Hall effect is explored. The MIR magneto-optical response shows very strong frequency dependence including sign changes. Below 200 meV, the MIR $\theta_H(T)$ changes sign between 120 and 150 K, as is observed in dc Hall measurements. Above 200 meV, the temperature dependence of θ_H is similar to that of the dc magnetization and the measurements are in good agreement with predictions from a band calculation for the intrinsic anomalous Hall effect (AHE). The temperature and frequency dependence of the measured Hall effect suggests that whereas the behavior above 200 meV is consistent with an intrinsic AHE, the extrinsic AHE may play an important role in the lower-energy response.

DOI: 10.1103/PhysRevB.81.235218 PACS number(s): 78.20.Ls, 78.66.Bz, 75.50.Cc, 75.47.Lx

I. INTRODUCTION

$Ca_xSr_{1-x}RuO_3$ compounds exhibit unusual properties, such as metamagnetism, quantum criticality, non-Fermi-liquid behavior, and an anomalous Hall effect (AHE) that continue to challenge the condensed-matter community. The Hall effect in $SrRuO_3$ consists of two parts, the ordinary Hall effect (OHE) due to a magnetic field B producing a Lorentz force on moving carriers and the AHE due to the sample's magnetization M. The Hall resistivity ρ_H is given by

$$\rho_H = \rho_{yx} = R_0 B + \rho_{yx}^{\mathrm{AHE}}(M). \tag{1}$$

The ordinary Hall coefficient R_0 is related to the carrier density. The anomalous Hall resistivity $\rho_{yx}^{\mathrm{AHE}}(M)$ can be divided into two categories: (1) the extrinsic AHE arising from impurity scattering and (2) the intrinsic AHE due to the band structure.[1] The anomalous Hall resistivity is expressed as

$$\rho_{yx}^{\mathrm{AHE}}(M) = R_s(\rho_{xx}) 4\pi M + \sigma_{yx}^I(M)\rho_{xx}^2, \tag{2}$$

where R_s is the extrinsic AHE coefficient as a function of the longitudinal resistivity ρ_{xx} and σ_{yx}^I is the intrinsic AHE transverse conductivity. The coefficient R_s contains two terms, one proportional to ρ_{xx} and one that varies as ρ_{xx}^2,

$$R_s(\rho_{xx}) = a\rho_{xx} + b\rho_{xx}^2, \tag{3}$$

where a and b are coefficients for two types of scattering processes. The first term is due to asymmetric (skew) scattering from impurities in the presence of magnetic order[2,3] and is considered to be a classical extrinsic effect. The second term is called "side-jump scattering" from impurities, which has a quantum-mechanical origin.[4–6] Note that although the side-jump scattering scales as ρ_{xx}^2 just as the intrinsic AHE, and some consider them to be equivalent, the latter is simply proportional to M while the former depends on M through the function $\sigma_{xy}^I(M)$. While the dc AHE is observed in many itinerant ferromagnetic materials ranging from ruthenates to colossal magnetoresistance oxides to diluted magnetic semiconductors, the degree to which its origin is intrinsic[6–10] or extrinsic[2,11] is still not resolved in many cases.[1] The dc AHE measurements by Ref. 11 suggest that the sign change in $\theta_H(T)$ occurs in $SrRuO_3$ when $\rho_{xx} = 107\ \mu\Omega$ cm. This behavior is consistent with the extrinsic AHE in Eq. (3), with the critical ρ_{xx} making $R_s = 0$ thereby producing a sign change in R_s.

There have been extensive dc measurements[11,12] to probe the temperature and magnetic field dependence of the Hall effect in $SrRuO_3$. There has also been a low-temperature study based on Kerr measurements to probe the frequency dependence of the Hall conductivity above 200 meV.[8] The work presented here is a systematic study of the temperature, magnetic field, and frequency dependence of the Hall response in $SrRuO_3$ in the 0.1–1.4 eV energy range. This range is particularly interesting since the only calculation to model the frequency ω dependence of the Hall conductivity σ_{xy} of $SrRuO_3$ predicts strong spectral features for σ_{xy} in this range.[8] This work provides the first experimental test of this model's predictions for $\sigma_{xy}(\omega)$ below 200 meV.

Conventional dc Hall-effect measurements in materials such as high-temperature superconducting cuprates (HTSC),[13] diluted magnetic semiconductors, and ruthenate perovskite materials have been essential in revealing the unusual character of these systems. Three major issues motivate the study of the midinfrared (MIR) AHE in these materials. The first and most general argument is that since the understanding of the dc AHE may be unresolved, studying the frequency dependence of the dynamic AHE can provide new information on the microscopic mechanisms that are responsible for the AHE. Second, MIR measurements[14]

would probe more effectively the energy scales of the system (e.g., the plasma frequency, the cyclotron frequency, and the carrier relaxation rates) and provide greater insight into the intrinsic electronic structure of a wide range of materials, including HTSC.[15–18] The MIR range is highly appropriate since the typical band energy scale for the AHE in diluted magnetic semiconductors,[7,19,20] $SrRuO_3$,[8] and other materials[21,22] is in the MIR. It is not surprising that the most striking spectral features in calculations of the AHE are in the MIR range. Unlike conventional MIR spectroscopy that measures the longitudinal conductivity σ_{xx}, which is related to the *sum* of the sample's response to left and right circularly polarized, MIR Hall measurements probe the Hall conductivity σ_{xy}, which is related to the *difference* in the sample's response to left and right circularly polarized light, and therefore is more sensitive to asymmetries such as spin splitting, etc. Finally, the dc Hall effect can be dominated by impurity-scattering or grain-boundary effects. This is especially important in new materials which often contain many impurities and defects. By probing the Hall effect at higher frequencies, the contribution from sample disorder can be minimized.

Magnetopolarimetry measurements can be used to extend Hall-effect measurements into the infrared frequency range (10^{13} Hz). These measurements are sensitive to the complex Faraday θ_F and Kerr θ_K angles, which are closely related to the complex Hall angle θ_H.[16] Since θ_H (and θ_F) obeys a sum rule[23] it is very useful to be able to integrate θ_H to higher frequencies to verify whether (and where) the Hall angle sum rule saturates or whether there is additional relevant physics at even higher frequencies. Finally, since the high-frequency behavior of θ_H is constrained by the general requirements of response functions, a simple, model-independent asymptotic form for θ_H becomes more accurate at higher frequencies.

In this paper, we report measurements of the MIR complex Faraday, Kerr, and Hall angles in $SrRuO_3$ films in the 0.1–1.4 eV energy range. The transmitted and reflected magneto-optical responses in the MIR are qualitatively similar to results from dc Hall and dc magnetization measurements. The measurements are in good agreement with predictions from a band calculation[8] above 200 meV. The deviations at lower energy are probably due to a stronger contribution from the extrinsic AHE.

II. EXPERIMENTAL SYSTEM

The Faraday and Kerr angles are measured using a sensitive polarization modulation technique[24–26] in the midinfrared and near-infrared (MNIR) spectral range (115–1400 meV) for a $SrRuO_3$ sample grown by pulsed laser deposition at Oak Ridge National Laboratory as described in Refs. 27 and 28. Several light sources such as various gas lasers, semiconductor lasers, and a custom-modified double pass prism monochromator with a Xe light source allow us to perform the measurement in a wide probe energy range. For details of the experimental technique see Refs. 24–26. The complex θ_F and θ_K angles are measured in the MNIR spectral range as a function of magnetic field up to 2 T and temperature from 10 to 300 K. The small background Faraday signal from the cryostat windows and the film substrate has been subtracted from the data. The complex conductivities σ_{xx} and σ_{xy} and the complex Hall angle θ_H are determined directly from the measured complex θ_F and θ_K using the analysis techniques in Ref. 25.

The dc longitudinal and Hall resistivities of $SrRuO_3$ were measured simultaneously using a four-probe van der Pauw geometry at UB's Magneto-Transport Facility as well as at Oak Ridge National Laboratory using a physical property measurement system (Quantum Design) in a six-terminal configuration and 1 mA currents.[27] Moreover, the film magnetization was measured by a superconducting quantum interference device magnetometer (Quantum Design) using a custom-modified sample holder, which enables measurements of the magnetization perpendicular to the film surface, which is the same configuration as our Faraday and Kerr measurements.

III. RESULTS

The Faraday and Kerr angles in $SrRuO_3$ were measured at various temperatures and a wide energy range to probe the AHE. The continuous broadband measurements allow us to extend θ_F and θ_K measurements up to 1.4 eV.[26] Although the intensity of broadband light is significantly weaker than that of lasers, and therefore the sensitivity is reduced, θ_F and θ_K are large and can be readily measured in this range. The analysis techniques to obtain the complex longitudinal (σ_{xx}) and transverse (σ_{xy}) conductivities and the NMIR Hall angles (θ_H) are based on the techniques in Ref. 25.

Figure 1 shows temperature dependence of θ_F and θ_K in $SrRuO_3$ as a function of applied magnetic field H at a photon energy of 117 meV. Both θ_F and θ_K exhibit ferromagnetic hysteresis until the remanent magnetization disappears at the Curie temperature $T_c \simeq 160$ K. Figure 1(a) presents $\mathrm{Re}(\theta_F)$ as a function of H at various temperatures. Note that the sign of the slope above 130 K is opposite of that observed at lower temperatures. Linear fits to the data at 150 and 160 K indicate nonmonotonic temperature behavior of the slope. The strongest change in $\mathrm{Re}(\theta_F)$ occurs below 1.5 T, where the ferromagnetic hysteresis loops close.

The Fig. 1(b) shows θ_F and θ_K as a function of H at 117 meV and 10 K. The magnitude of $\mathrm{Im}(\theta_K)$, which is not shown in Fig. 1(b), is an order of magnitude smaller than that of $\mathrm{Re}(\theta_K)$. Typically, for metallic films such as $SrRuO_3$ in the MIR, the magneto-optic response in transmission (θ_F) is larger than that obtained in reflection (θ_K), although the transmitted intensity of light can be as small as 0.01%, because $\theta_F \propto \sigma_{xy}/\sigma_{xx}$ while $\theta_K \propto \sigma_{xy}/(\sigma_{xx})^2$, where $\sigma_{xx} \gg \sigma_{xy}$ in metallic films.[25] For thicker and more metallic films, θ_F is much more sensitive to σ_{xy} than θ_K in the MIR. Therefore, measuring magneto-optic signals in both transmission and reflection with a higher sensitivity provides the measurements reported here with a distinct advantage over the technique used in Refs. 8 and 29, where only the reflected signal was measured. Moreover, the stronger θ_F signals are critical to explore the MIR Hall effect at higher temperatures, where the magneto-optical response is weaker.

It is not clear whether the sign change in $\mathrm{Re}(\theta_F)$ is due to a sign change in the AHE component or a linear OHE com-

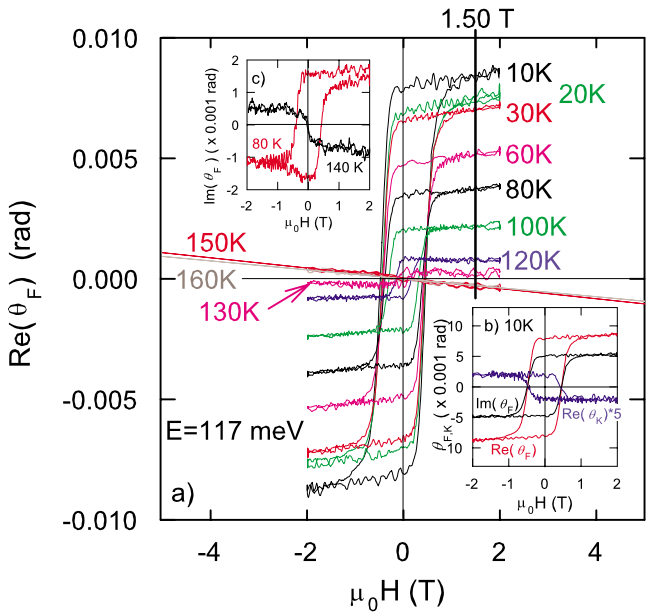

FIG. 1. (Color online) Temperature dependence of θ_F and θ_K from a $SrRuO_3$ film as a function of applied magnetic field H at a probe energy of 117 meV. The main panel (a) shows the temperature dependence of the hysteresis loops for Re(θ_F). Linear fits to the data at 150 and 160 K are also shown to help distinguish the data from other temperatures. The vertical line indicates H=1.5 T, where the hysteresis loops close at low temperatures. Inset (b) shows Re(θ_F), Im(θ_F), and Re(θ_K) (which is multiplied by a factor of 5) as a function of H at 117 meV and 10 K. Inset (c) shows the hysteresis loops for Im(θ_F) at 117 meV and two temperatures, 80 and 140 K, where the sign change near H=0 of Im(θ_F) is clearly seen.

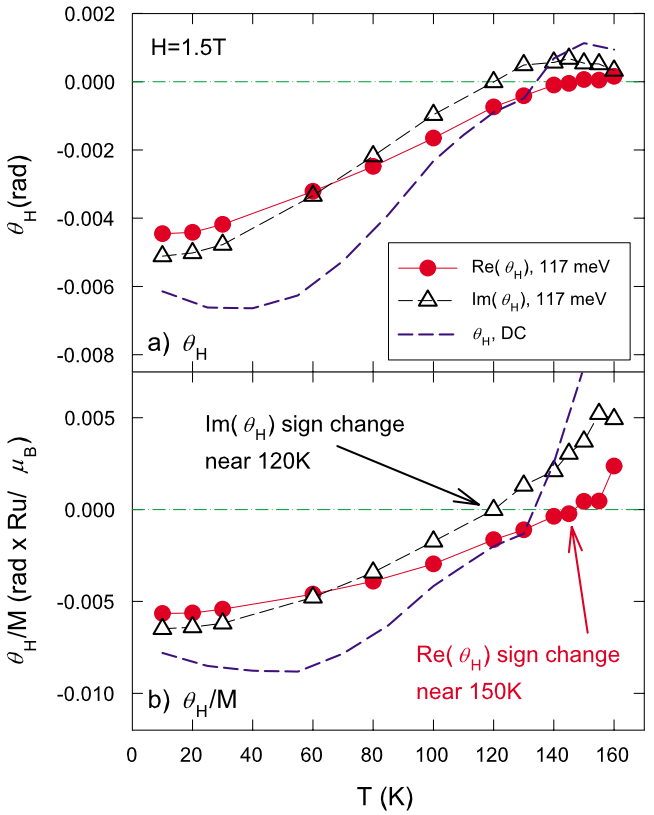

FIG. 2. (Color online) Temperature dependence of (a) $\theta_H(T)$ and (b) $\theta_H(T)/M(T)$ at 1.5 T at 117 meV and dc. The magnetization $M(T)$ is shown in Fig. 3.

ponent with opposite sign (from opposite charge carriers) which starts dominating at higher temperatures in Fig. 1(a). However, the AHE nature of the sign change is clearly seen in Fig. 1(c), which shows Im(θ_F) at 80 and 140 K at a probe energy of 117 meV. Here the sharp step near $H \simeq 0$ changes sign. The response of Re(θ_F) is linear in H at the sign change, which occurs in temperatures between 130 and 160 K, where the magnetization is smaller due to the proximity to T_c. On the other hand, unlike Re(θ_F), the sign change in Im(θ_F) appears between 80 and 140 K. The opposite signs for the hysteresis loop steps in Im(θ_F) indicate that the sign change is related to the magnetization, and hence due to a sign change in the AHE coefficient R_s. The sign change in the ferromagnetic step near H=0 is not clearly seen in dc Hall measurements, which demonstrates another advantage of magneto-optical measurements in probing AHE materials.

Figure 2 shows the Hall angle as a function of temperature at an applied magnetic field of 1.5 T and at a probe energy of 117 and 0 meV (dc). From θ_F and θ_K we obtain σ_{xx}, σ_{xy}, and $\theta_H = \sigma_{xy}/\sigma_{xx}$. Since the hysteresis loops close below $\mu_0|H| = 1.5$ T, this value of magnetic field is chosen to characterize the strength of the magneto-optical response. It is difficult to separate the OHE from the AHE above 1.5 T because both Hall signals are linear in H. Reference 30 has reported that the magnetization in $SrRuO_3$ does not saturate even at magnetic fields up to 40 T and found that the AHE signal can be linear in H up to 40 T. Although the separation of AHE from OHE has been done in dc measurements,[11] it is more challenging to make this separation for NMIR data. However, there are two regions where the OHE signal can be readily separated from the AHE signal. The first region is at lower temperatures and low magnetic fields, where magneto-optical response is ferromagnetic, θ_H is dominated by the AHE. For higher temperatures, it is difficult to separate AHE from OHE because the ferromagnetic response is weaker as the temperature increases toward T_c. The second region is at higher probe frequencies where the OHE is suppressed. The Drude model predicts that as the probe frequency ω increases past the characteristic scattering frequency γ_H, Re(θ_H) $\propto \omega^{-2}$ and Im(θ_H) $\propto \omega^{-1}$.[16] If one assumes that the linear part of the Hall angle ($\propto \theta_F$) above 1.5 T only comes from the OHE due to free carriers in Fig. 1, one can use the extended Drude model (EDM) to calculate the Hall frequency ω_H, which is related to the carriers' effective mass, and the Hall scattering rate γ_H.[16,17] Furthermore, one can estimate the maximum contribution of the OHE to the overall Hall response. The slope of the linear behavior of θ_F (and, therefore, θ_H) in Fig. 1 at fields above 1.5 T is nearly constant from 10 to 80 K. The slope translates into ω_H=−0.31 cm^{-1}/T (−0.039 meV/T) and γ_H=1102 cm^{-1} (137 meV). Assuming that the carrier scattering is isotropic, one can use ω_H to obtain a carrier effective mass of $2.99m_e$, where m_e is the bare electron mass. Since the Hall scattering rate γ_H is close to ω=117 meV, one expects that Re(θ_H) $\approx$ Im(θ_H)

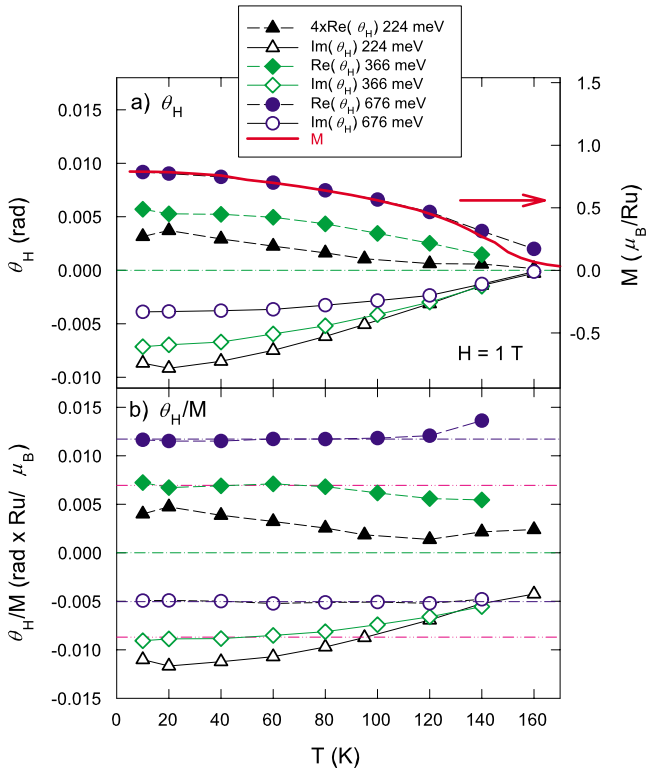

FIG. 3. (Color online) Temperature dependence of (a) $\theta_H(T)$ and $M(T)$ and (b) $\theta_H(T)/M(T)$ at 1 T above 200 meV. $\theta_H(T)$ is very similar to the magnetization $M(T)$ at 1 T. The horizontal lines in (b) are guide lines, which show $\theta_H(T) \propto M(T)$.

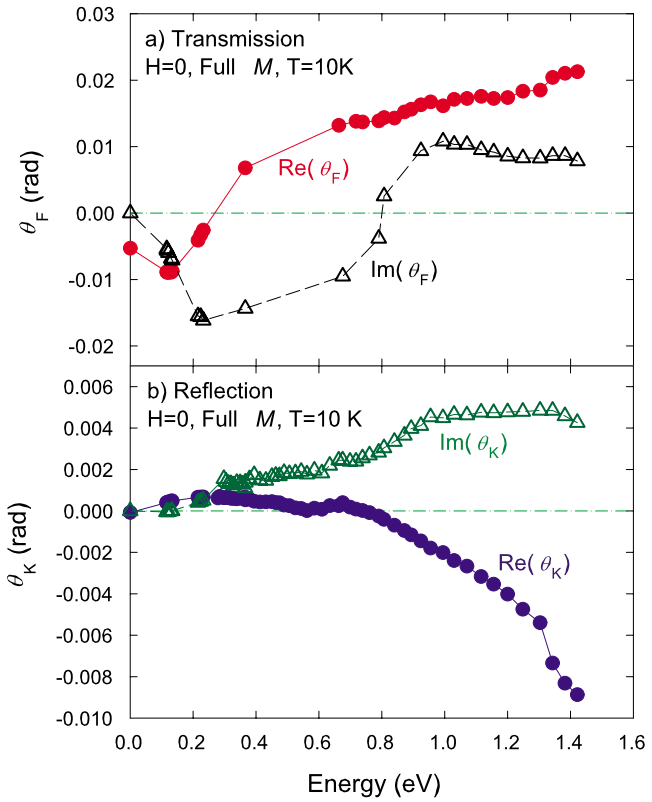

FIG. 4. (Color online) Energy dependence of the AHE (a) θ_F and (b) θ_K with the sample fully magnetized perpendicular to the plane at 0 T and 10 K. Since the measurement is at $H=0$ T, the OHE as well as background signals from the substrate and windows, which all are linear in H, do not contribute to the signal. At the energy range from 0.4–0.7 eV, the intensity of transmitted light is too weak to measure θ_F.

$\approx \omega_H/(2\gamma_H)$ when $\omega \approx \gamma_H$. The value of OHE given by the linear part of the hysteresis loops is less than 3% of the total Hall response below 80 K. Likewise, the OHE is much smaller at the higher frequencies over 117 meV due to $\omega \gg \gamma_H$.

Figure 2(a) shows the sign change in Re(θ_H) and Im(θ_H) at 117 meV near 130 K, where the Hall sign change is observed in dc measurements (dashed line). The magnitude and temperature behavior of θ_H at 117 meV and dc are very similar. The sign change in Im(θ_H) appears at a slightly lower temperature, deeper in the ferromagnetic phase, than Re(θ_H). It may explain why the sign change in Im(θ_F) [$\propto$Im(θ_H)] is more clearly seen in Fig. 1. The magnitudes of both Re(θ_H) and Im(θ_H) are slightly smaller than the dc value. The dc Hall angle exhibits a minimum value near 40 K but at 117 meV both Re(θ_H) and Im(θ_H) increase monotonically with temperature up to 120 K. Im(θ_H) at 117 meV rises more steeply than Re(θ_H), changes sign earlier, and reaches a maximum value near 140 K. Since the MIR Hall angles mostly come from the AHE, θ_H is dominated by the magnetization M. Figure 2(b) shows θ_H divided by the measured M, which is shown in Fig. 3(a) (solid line). The sign change in Re(θ_H)/M and Im(θ_H)/M is clearly seen. The sign change in Im(θ_H) occurs near 120 K and in Re(θ_H) near 150 K. These are symmetrically separated from the dc Hall sign change temperature.

Figure 3 shows the temperature dependence of the dc magnetization and θ_H at higher energies of 224, 366, and 676 meV, which is obtained from the formula $[\theta_H(+1T) - \theta_H(-1T)]/2$. In this case, $\theta_H(T)$ no longer changes sign as it does at 117 meV and dc measurements, instead $\theta_H(T)$ approaches zero gradually as shown in Fig. 3(a). As the probe energy increases, $\theta_H(T)$ behaves more like the magnetization M. The solid line in Fig. 3(a) represents the measured magnetization, which saturates at lower temperature to $0.8\mu_B$/Ru. At an energy of 676 meV, $M(T)$ and $\theta_H(T)$ exhibit the same temperature dependence over nearly the entire range as shown in Fig. 3(a). Typically, visible and near-infrared Faraday and Kerr measurements are used to determine the magnetization of materials. Figure 3(b) plots $\theta_H(T)/M(T)$ at higher energies of 224, 366, and 676 meV at 1 T. The horizontal guide lines show behavior where θ_H is proportional to M. At a probe energy 676 meV the value of θ_H/M is a constant at all temperatures but at 366 meV this is the case only at lower temperatures.

Figure 4 shows the anomalous Hall part of θ_F and θ_K at 10 K and 0 T with the sample fully magnetized out of plane as a function of probe energy. As seen before, the OHE contribution is small, especially at higher energies at $H \approx 1$ T. In addition, since the measurement is performed at $H=0$ T and OHE is proportional to H, the OHE cannot contribute to this Hall signal. Both θ_F and θ_K display a strong energy dependence and change sign mostly at lower energies but monotonically increase or remain fairly constant at higher energies

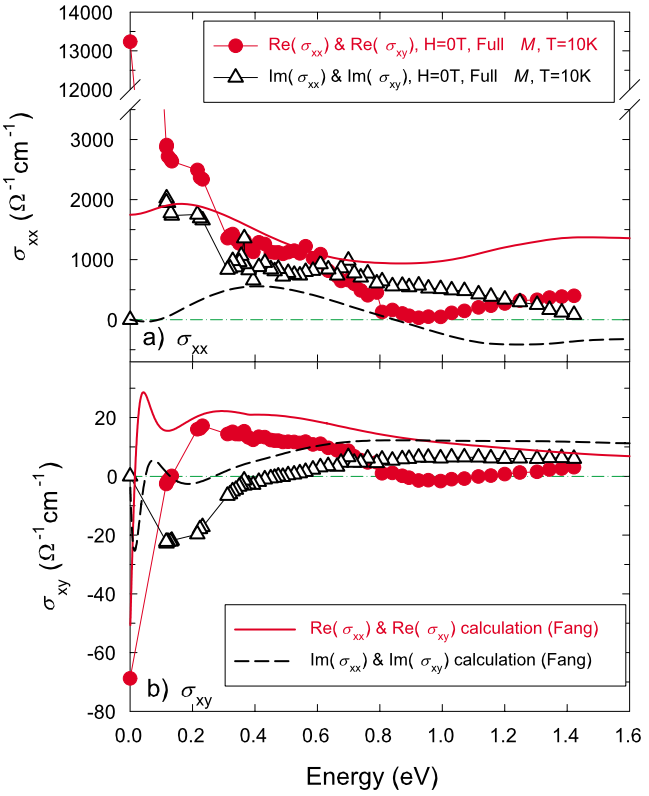

FIG. 5. (Color online) (a) The longitudinal conductivity σ_{xx} and (b) transverse (AHE) conductivity σ_{xy} as a function of probe energy. The thin lines are from a Berry phase calculation of the intrinsic AHE by Fang (Ref. 8). Note that this calculation neglects intraband transitions.

as shown in Fig. 4. The energy dependence of $\mathrm{Re}(\theta_F)$ and $\mathrm{Im}(\theta_K)$ is similar. The sign changes are observed at low energies near 250 meV for $\mathrm{Re}(\theta_F)$ and 130 meV for $\mathrm{Im}(\theta_K)$. Both signs change from negative to positive as energy increases. Note that the signs are defined and determined in Ref. 25. Likewise, $\mathrm{Im}(\theta_F)$ and $\mathrm{Re}(\theta_K)$ exhibit similar features. However, both sign changes appear near 800 meV. The sign of $\mathrm{Im}(\theta_F)$ also changes from negative to positive but the sign of $\mathrm{Re}(\theta_K)$ behaves oppositely. The dc values of θ_F and θ_K in Fig. 4 are determined in Ref. 25 and connect smoothly with the MIR data as $E \rightarrow 0$.

Figure 5 shows the measured and calculated complex (a) longitudinal conductivity σ_{xx} and (b) transverse (AHE) conductivity σ_{xy} as functions of probe energy. The symbols are obtained from θ_F and θ_K in Fig. 4 using the analysis techniques in Ref. 25. One advantage of determining both σ_{xx} and σ_{xy} from the same set of θ_F and θ_K measurements is that the behavior of σ_{xx}, which is well known in this energy range,[31] can be provide a consistency test for σ_{xy}, which is not well known. As experimentally seen in Ref. 25, the complex σ_{xx} from θ_F and θ_K is in good agreement over the entire energy range with σ_{xx} obtained from reflectance measurements on a different $SrRuO_3$ film.[31] Theoretical predictions for the AHE at finite frequencies have been limited. Although several different models are used to explain the dc AHE in $SrRuO_3$.[2,5,8,11] Here we compare the measured NMIR conductivities with predictions from an intrinsic AHE calculation for $SrRuO_3$.[8] The solid lines (the real parts of σ_{xx} and σ_{xy}) and dashed lines (the imaginary parts of σ_{xx} and σ_{xy}) are from a Berry phase calculation of the intrinsic AHE by Fang *et al.*[8] The calculated complex σ_{xx} in Fig. 5(a) clearly deviates from the measured σ_{xx}. This is not surprising since the model neglects intraband transitions, which play a dominant role at lower energies in a metal. For energies over 200 meV, the calculation agrees qualitatively and in some energy regions quantitatively with the measured values. Unlike the calculation, there is no sign change in the measured $\mathrm{Im}(\sigma_{xx})$ in our energy range.

Since the goal of this calculation was to provide insights into the behavior of σ_{xy}, it is encouraging that the agreement between the calculated and measured values of σ_{xy} is significantly better, as can be seen in Fig. 5(b). The Fang model predicts a sign change from electronlike at low energy to holelike at higher energies in both $\mathrm{Re}(\sigma_{xy})$ and $\mathrm{Im}(\sigma_{xy})$. The measured $\mathrm{Re}(\sigma_{xy})$ changes from electronlike for energies below 150 meV to holelike at higher energies. The measured $\mathrm{Im}(\sigma_{xy})$ appears to make the same change above 400 meV. Both $\mathrm{Re}(\sigma_{xy})$ and $\mathrm{Im}(\sigma_{xy})$ extrapolate smoothly to their dc values. Unlike conventional metals such as gold, which can be modeled using a single band in the infrared and where Drude behavior (intraband transitions) are responsible for the infrared Hall effect, in $SrRuO_3$ both intraband and interband transitions contribute, so the "electronlike" description is only meant to indicate signs, not the microscopic origin of the Hall effect. Of course, in the dc limit the OHE is solely due to intraband (Drude) behavior. Above 300 meV, the calculated $\mathrm{Re}(\sigma_{xy})$ and $\mathrm{Im}(\sigma_{xy})$ values run roughly parallel to the measured ones. In both the calculation and measurements, $\mathrm{Re}(\sigma_{xy})$ crosses $\mathrm{Im}(\sigma_{xy})$ at similar energies, near 0.8 eV for the measurements and 1 eV for the calculation. Below 300 meV, $\mathrm{Re}(\sigma_{xy})$ exhibits a peak near 200 meV in both the calculation and measurements. Another sharp peaklike structure is predicted in $\mathrm{Re}(\sigma_{xy})$ near 50 meV. However, the measured $\mathrm{Re}(\sigma_{xy})$ has already dipped below zero at 120 meV, in strong contrast to the theoretical upturn at 100 meV, and is heading toward the dc value smoothly. For $\mathrm{Im}(\sigma_{xy})$, the calculation and the measurements shows the zero crossing near 300 meV and 500 meV, respectively. As with the calculated $\mathrm{Re}(\sigma_{xy})$, the calculated $\mathrm{Im}(\sigma_{xy})$ also exhibits sharp peaks near 130 and 15 meV, but the slope and the large negative offset of the measured $\mathrm{Im}(\sigma_{xy})$ suggests that it will continue monotonically toward its dc value of zero. It is interesting to note that over the entire measured energy range, the calculated σ_{xy} generally agrees better with the data than the calculated σ_{xx}. These measurements strongly support the validity of the Berry phase model for describing the anomalous Hall response of $SrRuO_3$ above 200 meV but below 200 meV the measurements do not follow theoretical predictions.

Figure 6 shows the measured complex (a) Hall angle θ_H and (b) Hall resistivity ρ_H at 10 K and 0 T (sample fully magnetized out of plane). For low energies, $\mathrm{Re}(\theta_H)$ is nearly constant in the 0–120 meV range, whereas $\mathrm{Im}(\theta_H)$ increases linearly in the same range. The low-energy MIR θ_H measurements extrapolate smoothly to the dc values, suggesting that there are no additional features in the 0–120 meV range. Above 100 meV, $\mathrm{Re}(\theta_H)$ increases more rapidly with increasing energy, changes sign near 200 meV, and increases mono-

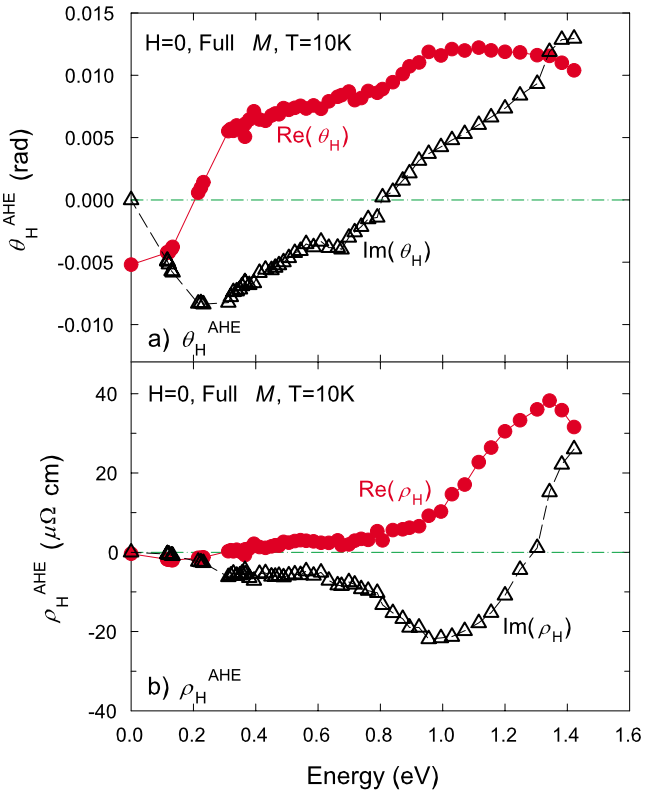

FIG. 6. (Color online) The complex (a) Hall angle θ_H and (b) Hall resistivity ρ_H at 10 K and 0 T with the sample fully magnetized out of plane as a function of probe energy. Since the measurement is at $H=0$ T, the signals are solely due to the AHE.

tonically over most of measurement range. Im(θ_H) reaches a minimum value near 200 meV, changes sign near 800 meV, and becomes more positive as energy increases. The energy dependence of ρ_H in Fig. 6(b) is nearly constant below 0.8 eV but above this energy the value of ρ_H increases an order of magnitude. Above 0.8 eV Re(ρ_H) has peak near 1.3 eV, where Im(ρ_H) changes sign. Additionally, Im(ρ_H) has a minimum value near 1 eV.

IV. DISCUSSION

Exploring the Hall effect in $SrRuO_3$ as a function of magnetic field H, temperature T, and frequency ω (or MNIR energy) can provide insights into this material as well as the AHE in general. We have seen that the MNIR θ_H (or σ_{xy}) is consistent with the predictions from an intrinsic AHE calculation for energy greater than 200 meV. On the other hand, the frequency, temperature, and magnetic field dependence below 200 meV may be more consistent with expectations from the extrinsic AHE. In this discussion, we explore the evidence for a crossover between intrinsic and extrinsic behaviors in the MIR energy range. Since the extended Drude model (EDM) was successfully applied to the IR σ_{xx} in $SrRuO_3$,[31] we will compare EDM predictions for σ_{xx} and σ_{xy} with our measurements in order to disentangle OHE and AHE contributions. Second, we apply a finite frequency extrapolation of the extrinsic AHE model to the temperature-dependent θ_H at 117 meV to test this model at and near dc.

The EDM is more important at lower energy because it models the intraband transitions which are dominant at and near dc. Note that the EDM considers the frequency-dependent relaxation time $\tau^*(\omega)$ and plasma frequency $\omega_p^*(\omega)$, which are renormalized by the mass enhancement factor $m^*(\omega)$. The longitudinal conductivity σ_{xx} is defined in EDM as

$$\sigma_{xx} = \frac{\omega_p^*(\omega)^2}{4\pi[\gamma^*(\omega) - i\omega]}, \tag{4}$$

where the renormalized scattering rate is $\gamma^*(\omega) = \tau^{*-1}(\omega) = \gamma(\omega)/m^*(\omega)$ and the frequency-dependent plasma frequency $\omega_p^*(\omega)^2 = \omega_p^2/m^*(\omega)$. The bare plasma frequency ω_p of the free-electron gas can be calculated by the carrier density. This model was used in $SrRuO_3$ to probe possible non-Fermi-liquid behavior exhibited in reflectance measurements.[31] It was reported that Re(σ_{xx}) falls like $\omega^{-0.5}$ and $\gamma^*(\omega)$ increases linearly with ω in the energy range between 0 and 1000 cm^{-1} (0–124 meV) at low temperature. The renormalized scattering rate is given by the formula $\gamma^*(\omega) = \omega[\mathrm{Re}(\sigma_{xx})/\mathrm{Im}(\sigma_{xx})]$, which is derived from Eq. (4). The scattering rate $\gamma^*(\omega)$ obtained from our σ_{xx} in Fig. 5(a) increases linearly with ω in the energy range of 116–600 meV (900–4800 cm^{-1}) and 10 K. Furthermore, in the same energy range the conductivity Re(σ_{xx}) drops like $\omega^{-0.68}$. Our results for σ_{xx} based on θ_F and θ_K measurements are consistent with that in Ref. 31.

The EDM allows one to extract the carrier density n of the electron gas. One way to obtain n is from the OHE. The Hall scattering parameters are extracted from the linear in H behavior of θ_H at low temperatures, assuming that this slope is solely due to the OHE. At 117 meV we obtain $\omega_H = -0.31$ cm^{-1}/T, $\gamma_H = 1102$ cm^{-1}, and a carrier effective mass of $2.99m_e$. Likewise, the MIR Hall coefficient R_H can be determined from the linear behavior of $\theta_H(H)$. The coefficient R_H is given by

$$R_H(\omega) = \frac{\rho_{yx}(\omega)}{B} = \frac{\theta_H(\omega)}{\sigma_{xx}(\omega)B}. \tag{5}$$

In a simple Drude model γ is constant, and $R_H(\omega)$ is purely real and constant. Considering only Re(R_H) at 117 meV, one can estimate $n = 1.04 \times 10^{22}$ electrons/cm^3 by using the formula $R_H = -\frac{1}{ne}$, where e is the electron charge. This value is nearly within a factor of 2 of that obtained in dc measurements by Khalifah *et al.*,[27] where $n = 2.5 \times 10^{22}$ electrons/cm^3 (or $n = 1.6 \times 10^{22}$ electrons/cm^3 from Ref. 32). This discrepancy is probably due to the fact that the linear behavior is not completely due to the OHE but also the AHE. If 50% of the net linear Hall angle signal at 117 meV between 1.5 and 2 T resulted from the AHE, leading to a factor of 2 decrease in the contribution from the OHE, the carrier density obtained from the slope of θ_H at 117 meV, at 10 K, and above 1.5 T would be 2.1×10^{22} electrons/cm^3. The carrier density $n = 1.04 \times 10^{22}$ electrons/cm^3 corresponds to a plasma frequency $\omega_p = 30\,517$ cm^{-1} while $n = 2.5 \times 10^{22}$ electrons/cm^3 corresponds to $\omega_p = 47\,315$ cm^{-1}. According to Ref. 31, the mass enhancement factor $m^*(\omega)$

approaches 1 as the energy exceeds 1000 cm^{-1}. This means that $\omega_p^*(\omega)^2 \approx \omega_p^2$ is satisfied from 1000 cm^{-1} up to 4800 cm^{-1}, where $\gamma^*(\omega) \propto \omega$. For the EDM σ_{xx}, the appropriate partial sum is

$$\frac{\omega_p^*(\omega_c)^2}{4\pi} = \int_0^{\omega_c} \frac{2}{\pi} \mathrm{Re}[\sigma_{xx}(\omega)] d\omega, \quad (6)$$

where ω_c is a cutoff frequency. To stay consistent with the analysis in Ref. 31, we fit the measured $\mathrm{Re}(\sigma_{xx})$ to the formula $A\omega^{-0.5}$, where A is a fitting parameter. If the partial sum is performed to $\omega_c = 1000$ cm^{-1}, then $\omega_p^* = 32\,636$ cm^{-1}, which corresponds to a carrier density $n = 1.2 \times 10^{22}$ electrons/cm^3. For $\omega_c = 4800$ cm^{-1}, $\omega_p^* = 48\,307$ cm^{-1}, which corresponds to $n = 2.6 \times 10^{22}$ electrons/cm^3. These values of carrier density are qualitatively in agreement with the values obtained from the OHE and dc measurements. The scattering parameters determined from the EDM reveal that intraband transitions play an important role in σ_{xx} below 100 meV.

As with the MIR $\sigma_{xy}(T)$, the behavior of θ_H can be divided into two distinct regions at 200 meV. Below 200 meV, the MIR $\theta_H(T)$ is similar to the dc $\theta_H(T)$ as in Figs. 2 and 3, but above 200 meV it looks like the dc magnetization $M(T)$. The agreement in $\sigma_{xy}(\omega)$ between the measurement and the strictly interband, intrinsic, Berry phase model at energies below 200 meV is not as good as at higher energies as shown in Fig. 5(b). Moreover, the EDM analysis suggests that intraband transitions are important to σ_{xy} and even more important to σ_{xx} at energies below 100 meV. One possible reason for the discrepancy between measurement and theory at low energies is that the lifetime broadening used in the calculation is too small for the $SrRuO_3$ film measured here, which exhibits much broader features. Another possibility is that the intrinsic model does not include intraband transitions, which play an important role near dc.

Since much of the dc AHE is commonly framed using Eqs. (1) and (3), it is interesting to study the temperature and frequency dependence of θ_H in terms of these equations. The simplest generalization to finite frequency of the extrinsic AHE θ_H is to simply use the frequency-dependent resistivity $\rho_{xx}(\omega)$ in Eqs. (1) and (3) at $H = B = 0$ T,

$$\theta_H(\omega) = \frac{\rho_H(\omega)}{\rho_{xx}(\omega)} = \frac{R_s(\omega)}{\rho_{xx}(\omega)} 4\pi M = [a + b\rho_{xx}(\omega)] 4\pi M. \quad (7)$$

Although this generalization is not rigorously correct, it can provide insight into the lower-energy AHE. If one considers only the extrinsic AHE at or near dc, the sign change in θ_H is due to a change in sign in R_s. In Ref. 11, the dc AHE always vanishes at the same value of $\rho_{xx}^* = 107$ $\mu\,\Omega$ cm, where $\theta_H(\rho_{xx}^*) = 0$, which suggests that the extrinsic AHE is dominant at dc. In our dc measurements, the sign change occurs at approximately $\rho_{xx}^* = 173$ $\mu\,\Omega$ cm. If one applies Eq. (7) using $\rho_{xx}(\omega)$ to the sign change at 117 meV, the sign change in $\mathrm{Re}(\theta_H)$ appears at $\rho_{xx}^* = 400$ $\mu\,\Omega$ cm and that of $\mathrm{Im}(\theta_H)$ occurs at $\rho_{xx}^* = 383$ $\mu\,\Omega$ cm. Typically, the longitudinal resistivity at 117 meV is two or three times larger than the value at dc because $\rho_{xx} \propto \gamma(\omega) \propto \omega$ at lower energies. According to Eq. (7), the sign change occurs when $\rho_{xx}^* = -a/b$. The parameters a (skew scattering) and b (side-jump scattering) are derived from microscopic origins.[2,3,5] The analysis at 117 meV reveals that a and b are energy dependent. Therefore, from $\rho_{xx}^*(\omega) = -a(\omega)/b(\omega)$ and since ρ_{xx}^* grows with ω, it could be interpreted that the skew scattering term $a(\omega)$ grows with respect to the side-jump scattering term $b(\omega)$ as energy increases for 0 to 117 meV. Another point of view is that the skew scattering is more sensitive to the probe energy than the side-jump scattering below 117 meV. Since the OHE is zero at $H = 0$ T or negligibly small even at $H \approx 0$ at the probe energy used here, the measured value is mostly contributed by the AHE.

V. CONCLUSION

To sum up the results, the intrinsic AHE model qualitatively agrees with the measurements above 200 meV and the disagreement between this model and the measurements at low energies is most likely due to the extrinsic AHE. There are several arguments to support the idea that the AHE in $SrRuO_3$ crosses over from extrinsic to intrinsic character as energy increases. First of all, although the origin of the AHE in $SrRuO_3$ is still not resolved and several papers[8–10] suggest that the AHE is intrinsic, other dc experimental papers[11,12] as well as our data below 200 meV suggest that the extrinsic AHE is important at low energy. Second, one would generally expect that as the driving frequency exceeds the impurity-scattering rate, the dominant contribution will no longer come from impurity scattering. At low frequency, the carriers scatter many times in each driving cycle, resulting in an AHE response that is primarily extrinsic. At high driving frequencies, the carriers oscillate many times before experiencing a scattering event, and hence the Hall response is dominated by the dynamics of the oscillations (band structure) and not by magnetic scattering. With an impurity-scattering rate on the order of 200 meV in $SrRuO_3$, one would expect the intrinsic AHE to start dominating the AHE above that energy. Note that the scattering rate obtained from EDM analysis of our IR conductivity measurements[31] is only a rough estimate that qualitatively guides our analysis. Third, the measured σ_{xy} agrees qualitatively with the intrinsic AHE model above 200 meV, where it runs close and nearly parallel to the calculated values. In fact, our σ_{xy} measurements above 200 meV agree with Fang's calculations better than the original data in Ref. 8, which are four times smaller than the calculated values. At lower energy the qualitative agreement between the calculation and our data worsens. The calculated $\mathrm{Re}(\sigma_{xy})$ flattens and may even begin to rise at 100 meV while the measured $\mathrm{Re}(\sigma_{xy})$ drops sharply at this energy. The calculated $\mathrm{Im}(\sigma_{xy})$ begins to rise at 100 meV, becoming positive, while the measured $\mathrm{Im}(\sigma_{xy})$ continues to become more negative at this energy. The dips in σ_{xy} near 100 meV predicted by the calculation may also be reflected in our data, but given the good tracking of the calculated and measured values above 200 meV, one could also argue that the data and calculations start to diverge more below 200 meV. Fourth, although we do not have data between dc and 100 meV, the data above 100 meV appear to extrapolate smoothly to their dc values, whereas the calculated values

are both heading away from the dc values at 100 meV. Unfortunately, our data cannot confirm nor rule out the predicted sharp peaks in this energy range. However, if the peaks in σ_{xy} occur near 50 meV, the measured dips near 100 meV would be significantly deeper than predicted by theory. One can make reasonable arguments that the extrinsic AHE becomes more important below 100 meV, and therefore a model based purely on the intrinsic AHE may have more limited accuracy in this range. Furthermore, band-structure calculations on $SrRuO_3$ are very sensitive to input parameters,[8,33] which makes the calculation of lower-energy structure very challenging. Fifth, the strong disagreement between the intrinsic model's predictions and experimental measurements for the longitudinal conductivity σ_{xx} in Fig. 5(a) clearly shows that free carriers (intraband transitions) are important below 200 meV. Although the quantitative agreement between the calculated and measured σ_{xx} above 200 meV is not as good, the energy dependence is roughly similar. However, the calculated $\mathrm{Re}(\sigma_{xx})$ flattens at a low value while the measured $\mathrm{Re}(\sigma_{xx})$ rises sharply to a much higher dc value. The calculated $\mathrm{Im}(\sigma_{xx})$ drops to zero quickly from 400 meV to dc while the measured $\mathrm{Im}(\sigma_{xx})$ is still increasing at 100 meV before dropping to the dc value of 0. The intrinsic model underestimates the dc $\mathrm{Re}(\sigma_{xx})$ by more than a factor of 6 as shown in Fig. 5(a). The EDM indicates clearly that the *intraband* AHE character (related to the impurity-scattering mechanism) is still significant compared with the *interband* AHE contribution near 100 meV, and even more important below 100 meV. Sixth, the temperature dependence of θ_H at 100 meV is strikingly similar to the dc behavior, as shown in Fig. 2(a). One can reasonably suggest that the 100 meV θ_H originates from the same mechanism as the dc θ_H, because they have similar magnitudes, similar temperature dependence, and change sign at a similar temperature. Although we cannot definitely rule out the intrinsic AHE near dc, if one accepts that the dc AHE is extrinsic one would generally expect to observe and our results may show a crossover to intrinsic behavior.

We suggest that our measurements may be probing two different regimes of the AHE in $SrRuO_3$, which is consistent with a crossover from the extrinsic to the intrinsic AHE near 200 meV. Unfortunately, we are not aware of any theoretical predictions on the energy dependence of the extrinsic AHE. Most experiments probing the AHE have been limited to exploring the temperature dependence of the dc AHE[9–12] or have looked at the low-temperature infrared AHE.[8] Our measurements have shown that energy as well as temperature is a critical parameter in understanding the AHE in $SrRuO_3$, and we hope that these experimental results will lead to new theoretical work on the AHE in $SrRuO_3$ in particular, as well as the extrinsic AHE in general.

ACKNOWLEDGMENTS

We thank K. Takahashi, A. J. Millis, N. P. Ong, and J. Sinova for helpful discussions. We also wish to thank B. D. McCombe for the use of UB's Magneto-Transport Facility. This work was supported by the Research Corporation Cottrell Scholar Grant; NSF-CAREER-DMR0449899, and the University at Buffalo, College of Arts and Sciences. Research at Oak Ridge National Laboratory was sponsored by the Division of Materials Sciences and Engineering, Office of Basic Energy Sciences, U.S. Department of Energy, under Contract No. DE-AC05-00OR22725 with Oak Ridge National Laboratory, managed and operated by UT-Batelle, LLC.

[1] N. Nagaosa, J. Sinova, S. Onoda, A. MacDonald, and P. Ong, Rev. Mod. Phys. **82**, 1539 (2010).
[2] J. Smit, Physica (Amsterdam) **21**, 877 (1955).
[3] J. Smit, Phys. Rev. B **8**, 2349 (1973).
[4] R. Karplus and J. M. Luttinger, Phys. Rev. **95**, 1154 (1954).
[5] L. Berger, Phys. Rev. B **2**, 4559 (1970).
[6] W.-L. Lee, S. Watauchi, V. L. Miller, R. J. Cava, and N. P. Ong, Science **303**, 1647 (2004).
[7] T. Jungwirth, Q. Niu, and A. H. MacDonald, Phys. Rev. Lett. **88**, 207208 (2002).
[8] Z. Fang, N. Nagaosa, K. S. Takahashi, A. Asamitsu, R. Mathieu, T. Ogasawara, H. Yamada, M. Kawasaki, Y. Tokura, and K. Terakura, Science **302**, 92 (2003).
[9] R. Mathieu, A. Asamitsu, H. Yamada, K. S. Takahashi, M. Kawasaki, Z. Fang, N. Nagaosa, and Y. Tokura, Phys. Rev. Lett. **93**, 016602 (2004).
[10] R. Mathieu, C. U. Jung, H. Yamada, A. Asamitsu, M. Kawasaki, and Y. Tokura, Phys. Rev. B **72**, 064436 (2005).
[11] Y. Kats, I. Genish, L. Klein, J. W. Reiner, and M. R. Beasley, Phys. Rev. B **70**, 180407(R) (2004).
[12] P. Khalifah, I. Ohkubo, B. C. Sales, H. M. Christen, D. Mandrus, and J. Cerne, Phys. Rev. B **76**, 054404 (2007).
[13] J. M. Harris, Y. F. Yan, and N. P. Ong, Phys. Rev. B **46**, 14293 (1992).
[14] H. D. Drew, S. Wu, and H.-T. S. Lihn, J. Phys.: Condens. Matter **8**, 10037 (1996).
[15] For example, see S. G. Kaplan, S. Wu, H.-T. S. Lihn, H. D. Drew, Q. Li, D. B. Fenner, J. M. Phillips, and S. Y. Hou, Phys. Rev. Lett. **76**, 696 (1996).
[16] J. Černe, D. C. Schmadel, M. Grayson, G. S. Jenkins, J. R. Simpson, and H. D. Drew, Phys. Rev. B **61**, 8133 (2000).
[17] J. Černe, M. Grayson, D. C. Schmadel, G. S. Jenkins, H. D. Drew, R. Hughes, A. Dabkowski, J. S. Preston, and P.-J. Kung, Phys. Rev. Lett. **84**, 3418 (2000).
[18] A. Zimmers, L. Shi, D. C. Schmadel, W. M. Fisher, R. L. Greene, H. D. Drew, M. Houseknecht, G. Acbas, M.-H. Kim, M.-H. Yang, J. Cerne, J. Lin, and A. Millis, Phys. Rev. B **76**, 064515 (2007).
[19] J. Sinova, T. Jungwirth, J. Kucera, and A. H. MacDonald, Phys. Rev. B **67**, 235203 (2003).
[20] G. Acbas, M.-H. Kim, M. Cukr, V. Novák, M. A. Scarpulla, O. D. Dubon, T. Jungwirth, J. Sinova, and J. Cerne, Phys. Rev. Lett. **103**, 137201 (2009).
[21] S. Broderick, L. Degiorgi, H. R. Ott, J. L. Sarrao, and Z. Fisk,

Eur. Phys. J. B **27**, 3 (2002).
[22] Y. P. Sukhorukov, E. A. Ganshina, B. I. Belevtsev, N. N. Loshkareva, A. N. Vinogradov, K. D. D. Rathnayaka, A. Parasiris, and D. G. Naugle, J. Appl. Phys. **91**, 4403 (2002).
[23] H. D. Drew and P. Coleman, Phys. Rev. Lett. **78**, 1572 (1997).
[24] J. Černe, D. C. Schmadel, L. B. Rigal, and H. D. Drew, Rev. Sci. Instrum. **74**, 4755 (2003).
[25] M.-H. Kim, G. Acbas, M.-H. Yang, I. Ohkubo, H. Christen, D. Mandrus, M. A. Scarpulla, O. D. Dubon, Z. Schlesinger, P. Khalifah, and J. Cerne, Phys. Rev. B **75**, 214416 (2007).
[26] M. Kim, V. Kurz, G. Acbas, C. Ellis, and J. Cerne, arXiv:0907.3128 (unpublished).
[27] P. Khalifah, I. Ohkubo, H. M. Christen, and D. G. Mandrus, Phys. Rev. B **70**, 134426 (2004).
[28] I. Ohkubo, H. M. Christen, S. Sathyamurthy, H. Y. Zhai, C. M. Rouleau, D. G. Mandrus, and D. H. Lowndes, Appl. Surf. Sci. **223**, 35 (2004).
[29] Science supporting online materials for Ref. 8 available at www.sciencemag.org
[30] T. Kiyama, K. Yoshimura, K. Kosuge, H. Mitamura, and T. Goto, J. Phys. Soc. Jpn. **68**, 3372 (1999).
[31] P. Kostic, Y. Okada, N. C. Collins, Z. Schlesinger, J. W. Reiner, L. Klein, A. Kapitulnik, T. H. Geballe, and M. R. Beasley, Phys. Rev. Lett. **81**, 2498 (1998).
[32] M. Izumi, K. Nakazawa, Y. Bando, Y. Yoneda, and H. Terauchi, J. Phys. Soc. Jpn. **66**, 3893 (1997).
[33] G. Santi and T. Jarlborg, J. Phys.: Condens. Matter **9**, 9563 (1997).